JOURNAL OF AIRCRAFT
Vol. 39, No. 5, September–October 2002

Computational-Fluid-Dynamics Based Advanced Ship-Airwake Database for Helicopter Flight Simulators

M. C. Bogstad,* W. G. Habashi,† I. Akel,‡ and D. Ait-Ali-Yahia§
Newmerical Technologies, Int., Montreal, Quebec H3A 2M7, Canada
and
N. Giannias¶ and V. Longo**
CAE Electronics Ltd., Montreal (VSL), Quebec H4L 4X4, Canada

Computational fluid dynamics (CFD) is used to create an extensive aerodynamic ship-airwake database for a ship-specific flight simulator to train helicopter pilots for landing and takeoff from various points on a ship. The technology has been embedded into CAE's Merlin simulator and applied to six different ships of the Royal Navy. In achieving this, important scientific and engineering milestones are crossed, including high geometric fidelity through OEM's (Original Equipment Manufacturer) CAD description of the ships, three-dimensional CFD calculations, comparison to experimental data, and, finally, integration, testing, and acceptance into the flight simulator. The database is first built by solving the three-dimensional inviscid (Euler) flow around the complete ship, using Finite Element Navier–Stokes Analysis Package, a proprietary code. And a number of wind speeds and directions, corresponding to realistic approach scenarios, are analyzed. The CFD results are then compared to a set of experiments carried out for airwakes around the Canadian Patrol Frigate and made available only after the calculations were done. The calculations prove to be in excellent agreement with the data throughout its range. For the purpose of integration into the simulator, the CFD solutions are interpolated onto a Cartesian grid, which is then implemented in a look-up table for the Merlin CDS, after being enhanced with turbulence models. The paper then closes with the acceptance procedure the simulator is passed through.

I. Introduction

COMPUTATIONAL fluid dynamics (CFD) is playing a growing, if not major, role in the aerodynamic design of most civil and military aircraft. The rapid evolution in computational power and in sophistication of algorithmic tools allows accurate prediction of airflow and a corresponding reduction in testing.

For various reasons, not least among them the proprietary and sensitive nature of an aircraft manufacturer's data, CFD has rarely, if ever, been used as a basis for constructing a flight simulator. The present work is part of a concerted effort to bring CFD into the fore into the area of flight simulators for pilot training. Two problems of current concern in terms of safety are being actively tackled: the first being the training for helicopter landing on ships, and the second being training for handling and performance events caused by in-flight icing,[1] for which Newmerical Technologies is also involved in developing a modern aerodynamic database.

The advantages of using simulators for training are self-evident (no risk, lower cost, greater availability, etc.). Continuous advances in computer power have caused leaps in the fidelity of representing real-time complex models and bringing flight simulation to its current virtual reality state. This increase in realism has, naturally, led to an expansion of the training tasks that can be performed on a simulator. With the two processes, more realistic simulation and expanding tasks, feeding on one another, the anticipation is that traditional simulation will not only grow rapidly but will also filter through to the aerodynamic design process proper. It should not be long before design engineers can play in real time, safely on desktop computers, a wide range of flight scenarios. This will lead to increased safety, and eventually to a concept of virtual certification, by enabling aerodynamicists to explore scenarios outside the envelope. Flight simulation, in this broader sense, will thus increasingly become an integral part of the entire cycle of conceptualization—design—certification—sales—support, with aircraft manufacturers naturally directly getting involved into the training process.

Although the visual and dynamic features of flight simulators have advanced tremendously in terms of realism, their "aerodynamic heart," however, continues to use empirical rules that, although easy to implement, might be inadequate in representing flowfields around complicated structures or at off-design conditions. It is only recently that CFD could be contemplated for an aerodynamic database of the flowfield around Royal Navy ships. Although CFD is certainly not directly applicable to real-time simulation, its results can as easily be integrated into the same type of look-up tables as empirical rules. CFD is still wrongly perceived as being expensive and inaccurate. Given the rapid advances in speed, algorithms, and capabilities, CFD cost now pales in comparison to experimentation, and its detailed renditions shine against empirical rules.

Thus, a CFD database is proposed to determine the aerodynamic effects on a helicopter on its final landing approach on a ship. The techniques used to obtain the database and the challenges associated with implementing the CFD solutions are described. Added realism is achieved in a cost-effective manner by addressing the relevant CAD issues and CFD methodology, through inviscid solutions plus added turbulence, unstructured grids.

Numerical results are presented and discussed in detail for five Royal Navy ships. The process is then carried out to its eventual engineering end: the database is placed in the simulator, and the methodology for validation and the pilots' evaluation are described.

Received 15 November 2000; revision received 27 February 2002; accepted for publication 28 February 2002.

*Engineer, 680 Sherbrooke West, 7th Floor; currently Engineering Specialist, Bombardier Aerospace, Advanced Aerodynamics Group, P.O. Box 6087, Montreal, Quebec, Canada H3C 3G9.
†President NIT, 680 Sherbrooke West, 7th Floor.
‡Engineer, 680 Sherbrooke West, 7th Floor.
§Engineer, 680 Sherbrooke West, 7th Floor; currently Staff Engineer, Multi-Disciplinary Numerical Methods, Pratt and Whitney Canada, Longuenil, QC Canada J4G 7A7.
¶Manager, Sensor Systems, 6585 Côte de Liesse.
**Group Leader, Aerodynamics and Propulsion, Military Flight Systems, 6585 Côte de Liesse.

II. Numerical Formulation

The prohibitive costs of an unsteady viscous flow analysis over a complete ship may be a bit of an overkill[2] in terms of cost. It is considered here that, as a first step in introducing more realism into a flight simulator through numerical simulation, a combination of an Euler solution and modeled unsteadiness[3,4] might be the appropriate level of complexity for a cost-effective solution with reasonable resources.

To this end, the inviscid (Euler) equations of motion are solved in this paper. They are implemented in a proprietary code Finite Element Navier–Stokes Analysis Package (FENSAP), whose governing equations, stated in their conservative form are as follows:

Continuity:

$$\frac{\partial \rho}{\partial t} + (\rho v_i)_{,i} = 0 \tag{1}$$

The semidiscretized form of the governing equations is obtained by applying the Galerkin finite element method in space. Equal-order interpolation is used for all variables:

Momentum equations:

$$\frac{\partial \rho v_i}{\partial t} + (\rho v_i v_j)_{,j} = -p_{,j} \tag{2}$$

Equation of state:

$$p = \rho R T \tag{3}$$

where ρ, v, t, p, R, T are density, velocity, time, pressure, universal gas constant, and temperature, respectively.

The odd-even decoupling associated with solving the preceding set of equations is suppressed by adding artificial terms, namely, a pressure dissipation term in the continuity equation and an artificial viscosity term in the momentum equation. The pressure dissipation term $\lambda\nabla^2 p$ added to the right-hand side of the continuity equation, changes the equation to

$$\frac{\partial \rho}{\partial t} + \nabla\cdot(\rho \boldsymbol{V}) = \lambda\nabla^2 p \tag{4}$$

To stabilize the solution of the momentum equations, an artificial dissipation (viscosity), proportional to the Laplacian of the velocity, is introduced:

$$\nabla\cdot(\rho V V) + \nabla p - \varepsilon_1 \nabla^2 V = 0 \tag{5}$$

Even though good results can been obtained by using Eqs. (4) and (5), the penalty is that conservation of mass and momentum can only be achieved within an error proportional to the pressure dissipation (continuity) and artificial dissipation (momentum) terms. These effects must therefore be minimized, and one way of doing this is by making the equations second-order-accurate. For example, for the continuity equation one writes

$$\frac{\partial \rho}{\partial t} + \nabla\cdot(\rho \boldsymbol{V}) = \lambda\nabla\cdot(\nabla p - \overline{\nabla p}) \tag{6}$$

where the balancing term $\overline{\nabla p}$ represents the nodal values of the averaged gradients of pressure. More details of the second-order artificial viscosity scheme for the momentum equations can be found in Ref. 5.

The steady-state solution is computed by marching in time, and a Newton method is then used to linearize the resulting equations. Highly parallelized preconditioned iterative solvers on shared memory machines, such as Generalized Minimal Residual, are used for solving the continuity and momentum equations in a fully coupled way. The energy equation is solved for the total temperature in a segregated manner. The resulting set of simultaneous linear equations, at each Newton step for p and $\rho\boldsymbol{V}$, can symbolically be written as

$$\begin{bmatrix} [M]/\Delta t + [K^V]_V & [K^p]_V \\ [K^V]_p & [M]/RT\Delta t + [K^p]_p \end{bmatrix} \begin{bmatrix} \Delta\rho\boldsymbol{V} \\ \Delta p \end{bmatrix} = -\begin{bmatrix} R_V \\ R_p \end{bmatrix} \tag{7}$$

where $[K]$ is the influence matrix and R_V and R_p represent the residuals of the momentum and continuity equations, respectively.

The solution procedure involves a series of steps in which the artificial dissipation in the numerical scheme is progressively unloaded by decreasing values of the pressure dissipation and artificial viscosity parameters. The solutions are considered converged when a reduction of four orders in the L-2 residual of each of the Euler equations is reached, using the smallest amounts of pressure dissipation and artificial dissipation possible.

III. Test Cases and Boundary Conditions

A. Selection of Test Cases

In this paper five Royal Navy ships are presented, along with their flow conditions (see Table 1): 1) Canadian Patrol Frigate (CPF), presented in Fig. 1; 2) Type 22 Broadwood Class (Batch 3)—Cumberland, presented in Fig. 2; 3) Argus (ATS), presented in Fig. 3; 4) Invincible Class-Ark Royal, presented in Fig. 4; and 5) LPH Ocean, presented in Fig. 5.

B. Topology and Meshing Strategy

The computational domain consists of a cylinder in which the boat is embedded. The radius of the cylinder is at least four and half times the ship's length, whereas its height is approximately three ship lengths.

On the outer wall of the cylinder, an inlet and an exit region are defined on which boundary conditions are imposed. The inlet region is a 270-deg wedge aligned perpendicular to the incoming

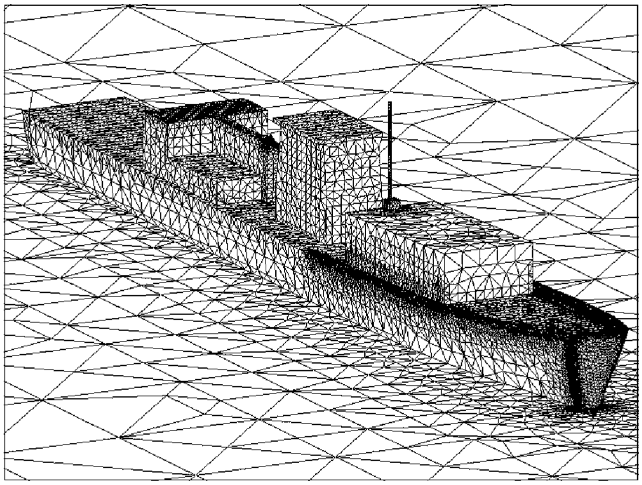

Fig. 1 Tetrahedral surface mesh and sea-level of the Canadian Patrol Frigate.

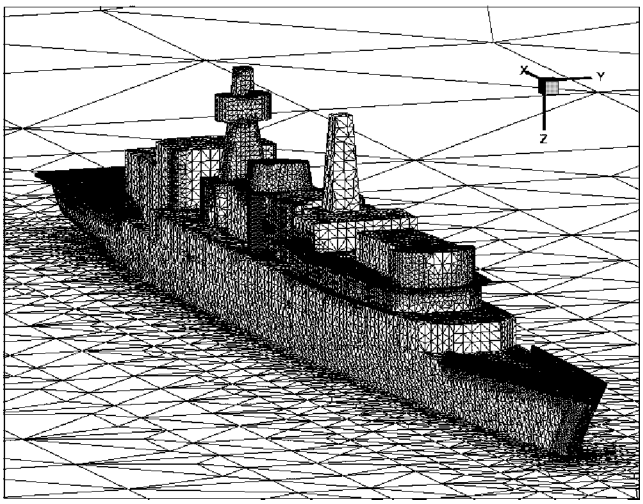

Fig. 2 Tetrahedral surface mesh and sea-level of the Cumberland.

Table 1 Wind directions table

Ship	Wind angle to ship α, deg (all cases at 40 kts)
Canadian patrol frigate	0
Cumberland	0, 30, 60, 90, 135, 180
Argus	0, 30, 60, 90, 135, 180, 225, 270, 315
Ark royal	0, 30, 60, 90, 135, 180, 225, 270, 315
LPH ocean	0, 45, 90, 135, 180, 225, 270, 315

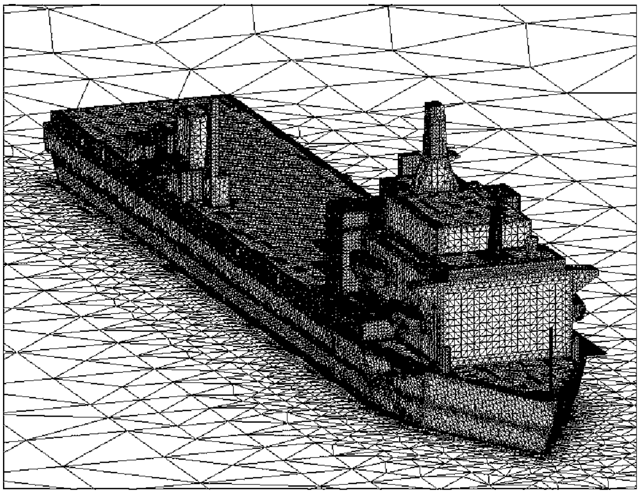

Fig. 3 Tetrahedral surface mesh and sea-level of the Argus.

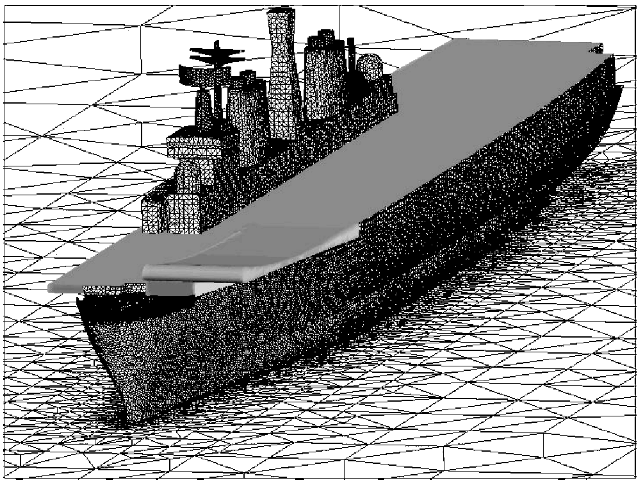

Fig. 4 Tetrahedral surface mesh and sea-level of the Ark Royal.

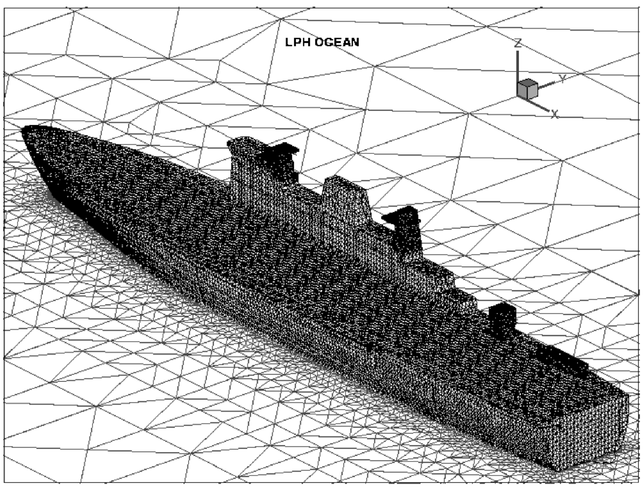

Fig. 5 Tetrahedral surface mesh and sea-level of the LPH Ocean.

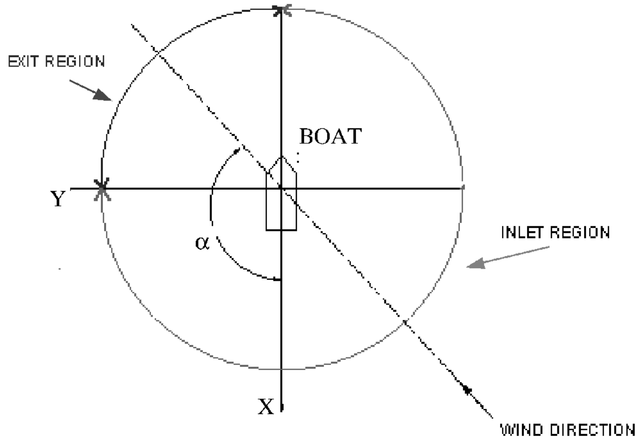

Fig. 6 Top view of typical computational domain with inlet and exit region indicated.

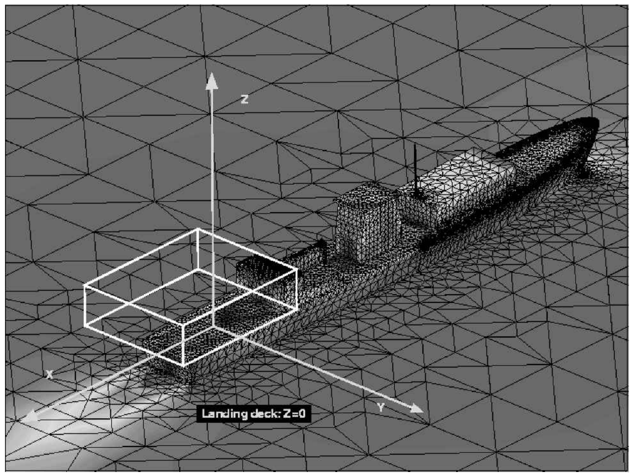

Fig. 7 Indication of the experimental domain.

wind direction, whereas the remaining 90-deg wedge forms the exit region and completes the cylinder (Fig. 6). In our inviscid flow simulations the surface of the sea has been treated as a solid wall. The top of the cylinder is defined as an inlet region.

Both block-structured hexahedral and unstructured tetrahedral meshes were created with the commercial mesh generation package ICEM-CFD. Our analysis has shown that for inviscid flow simulations the advantages, in terms of mesh generation time, of tetrahedral meshes vs hexahedral meshes are great, and hence only results on tetrahedral meshes are presented.

IV. CFD Experimental Validation on the Canadian Patrol Frigate

Validation test cases for flow over ships are rare and, when available, are proprietary to various governments. Thus, it was extremely fortunate that this particular Canadian Patrol Frigate test case was made available by the National Research Council of Canada[6] as a validation between for CFD calculations.

The calculations were carried out blind, that is, the experimental data were only made available to the authors only after the calculations were made.

The experiments were carried out in a box region positioned above the aft landing (Fig. 7). In the comparison presented in this paper, the so-called fixed probe data were compared to the velocity predicted by the FENSAP code.

Figure 8 shows the top view of the landing deck at different heights (that is, 4, 8, and 12 m) above the landing deck. The flow in the figure is from left to right, and one can clearly identify the wake on the deck created by the superstructure. A qualitative comparison between the experimental data (top row) with the corresponding numerical data

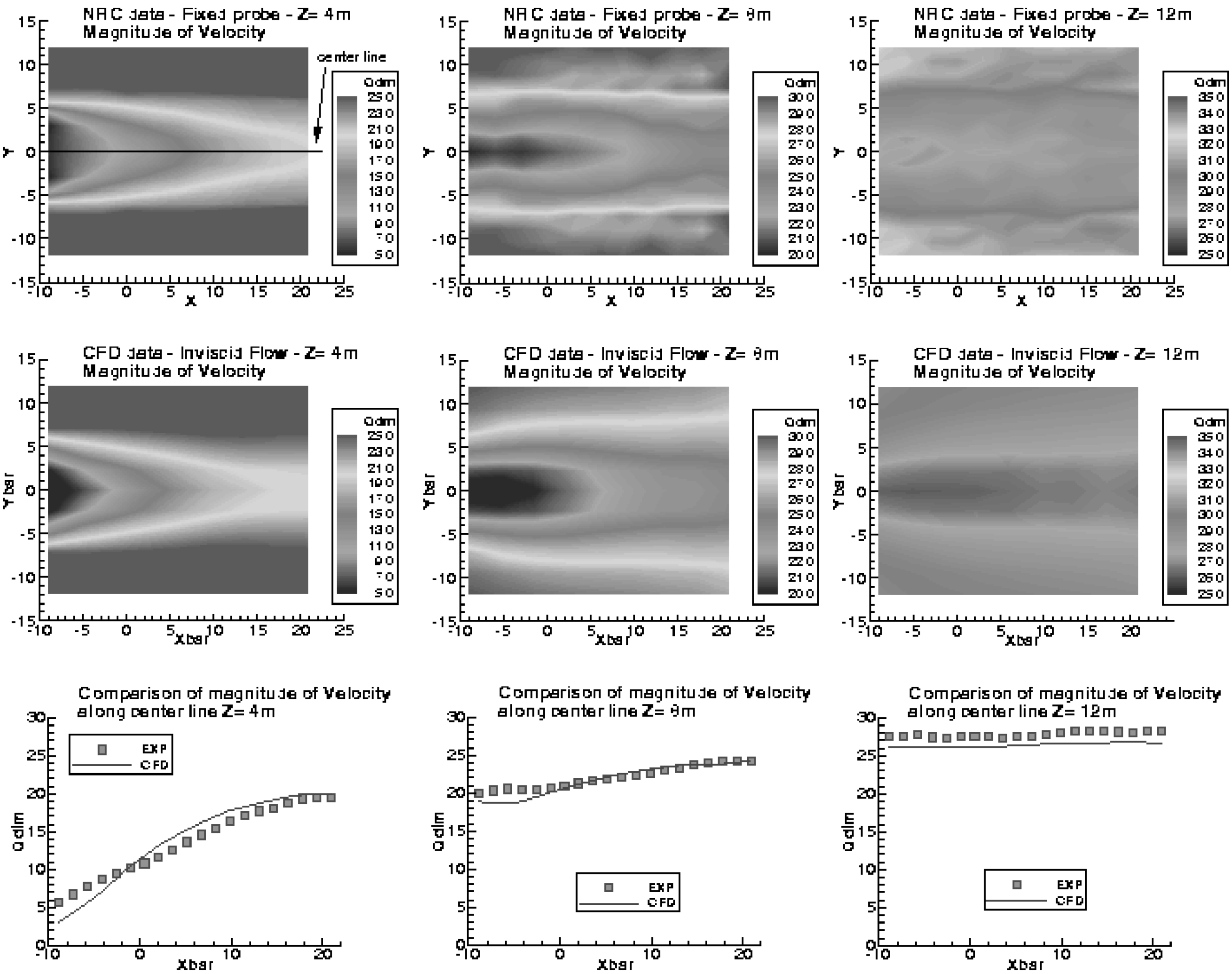

Fig. 8 Comparison between experimental data and FENSAP results, at different heights.

(middle row) shows a remarkably good agreement, considering the assumption of inviscid flow. A more detailed comparison is then made along the centerline of the deck (bottom row). Again, the agreement is excellent. The numerical solution's slight waviness at 8 and 12 m above the deck is mainly caused by the relative coarseness of the mesh at these levels.

A similar analysis was made in the streamwise direction (Fig. 9), and three planes are examined ($x = -8.928$, 5.952, and 20.832 m). The flow in the figure is coming toward the reader, and similar conclusions can be drawn. The numerical data compare remarkably well with the experimental data and fully capture the nature of the flow behind the superstructure, both at deck level and higher. As was done in the prceding comparison, the measured and predicted flows along the deck's centerline were compared.

V. Complete Numerical Results

A. Cumberland

Figure 10 represents the Mach-number contours on the landing deck of the Cumberland. The flow angle α for this case is 30 deg. To enhance the flow features on the landing deck, streamlines are added. Note the sharp region dividing the landing deck in a high-Mach-number region (red hue) and a low-Mach-number region (blue hue). On the hangar door a vortex structure can be observed.

B. Argus

The results of the Argus are presented in Figs. 11 and 12. Figure 11 shows pressure contours in the plane of symmetry. The main interest is the helicopter landing deck and results are displayed on the deck only but have, of course, been calculated over the entire ship and beyond (Fig. 12). The bow of the ship is located on the left side of the graphs, and its stern is located on the right of the graphs (see arrows). The large rectangular white region just right of center corresponds to the control tower area. The small white areas on the left correspond to a crane and lift shafts. The figures show the Mach-number variation for different wind directions, and, as before, streamlines have been added. The following observations can be made:

1) $\alpha = 0$ deg. The flow is, as expected, symmetric until it meets the control tower section. Because of the presence of the bridge/quarter section, a pair of counter-rotating vortices are generated behind it. One of the vortices coincides with a helicopter landing strip, and such flow conditions could pose difficulties for safely landing.

2) $\alpha = 30$ deg. As the flow comes in at an angle, it is accelerated between the bridge/quarter section and the control tower. As can be seen with comparison to the other graphs, it will produce the highest velocity (most red color) on the landing deck of all cases examined. No vortex structures are, however, present.

3) $\alpha = 60$ deg. A similar type of flow pattern as the 30-deg case exists, although velocities are not as high. However, a vortex structure can be observed, created by the control tower section and partly covering a helicopter landing deck. Again, such vortices could prove hazardous for landing.

4) $\alpha = 90$ deg. The flow from the side creates two counter-rotating vortices behind the control tower section and covers a helicopter landing strip. An approach, for example, along the centerline of the deck, could prove extremely difficult as a result of the

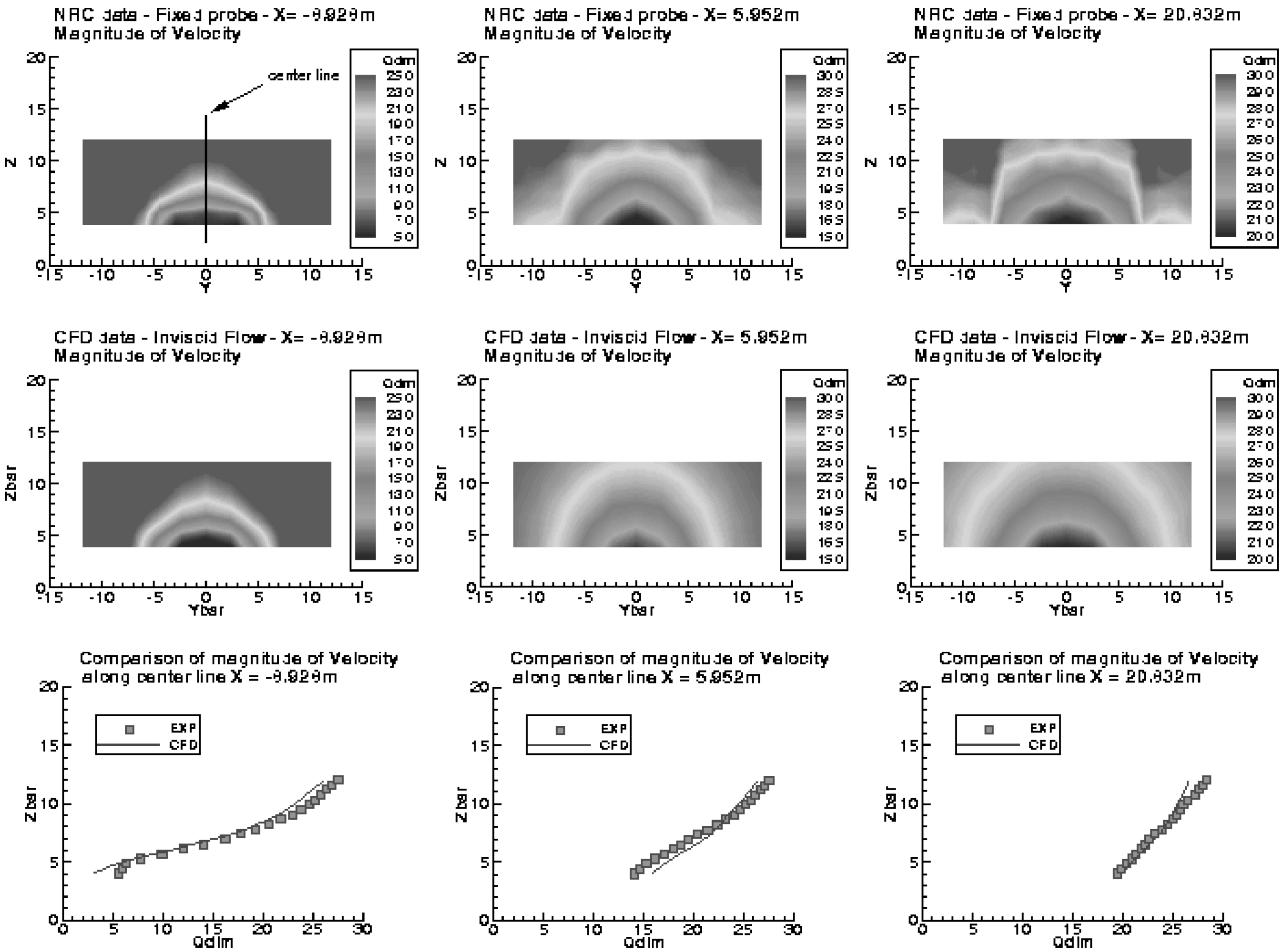

Fig. 9 Comparison between experimental data and FENSAP results in the streamwise direction.

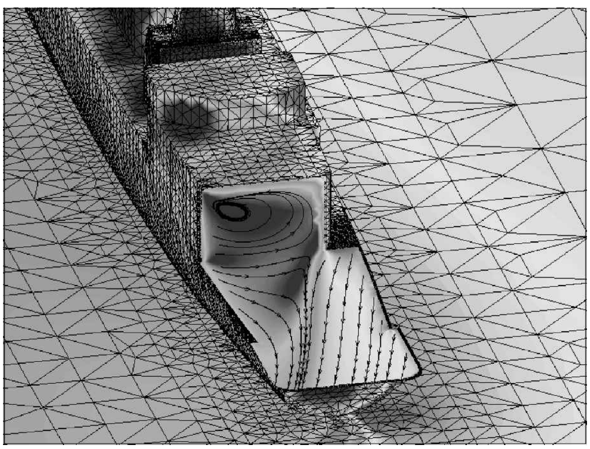

Fig. 10 Mach-number contours and selected streamlines on the landing deck of the Cumberland for α = 30 deg.

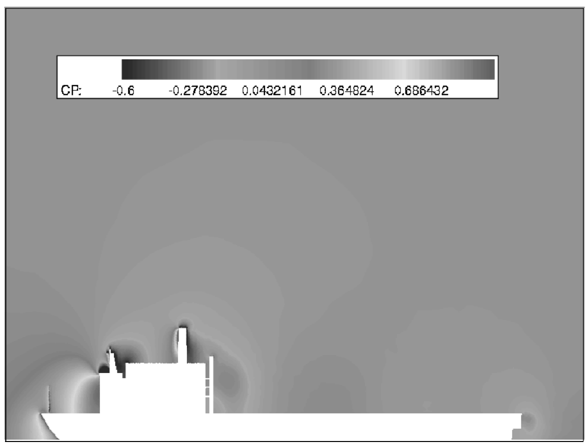

Fig. 11 Pressure contours in the plane of symmetry of the Argus for α = 0 deg.

presence of these vortices. The magnitude of the velocity is relatively small.

5) $\alpha = 135$ deg. The wind from the rear gives rise to high velocities, and no vortex structures are present.

6) $\alpha = 180$ deg. There is a very symmetric flow pattern, low velocities, and no vortex structures present.

7) $\alpha = 225$ deg. There are medium high velocities, and no vortices are present.

8) $\alpha = 270$ deg. There are low velocities, and no vortex structures are present.

The analysis shows that, under certain conditions, vortex structures are generated on landing strips of the deck. Such structures could prove hazardous for helicopter pilots. The vortices are generated as a result of pressure differences in the wake of an obstruction such as the control tower section or bridge/quarters section. It is therefore very unlikely that such vortices are present further away in

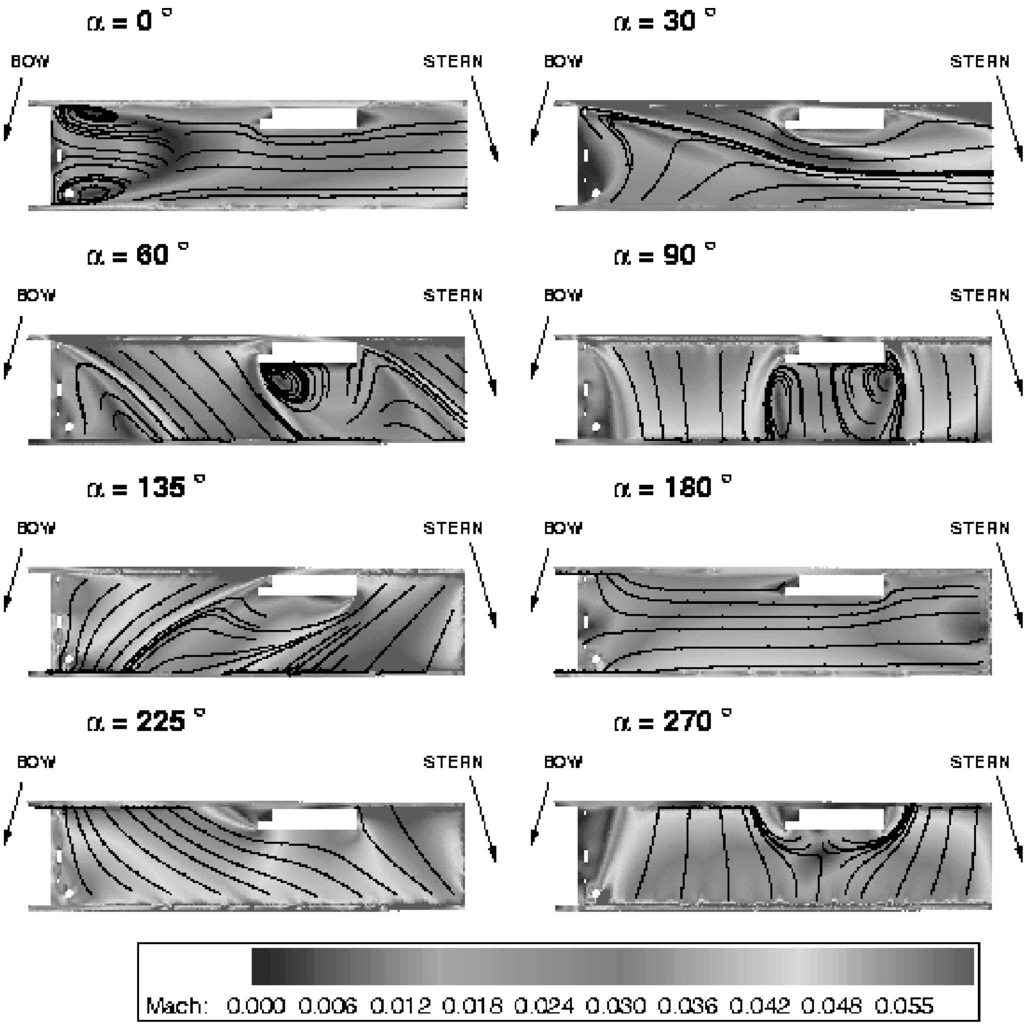

Fig. 12 Iso-Mach contours and selected streamlines on landing deck of the Argus for different wind directions.

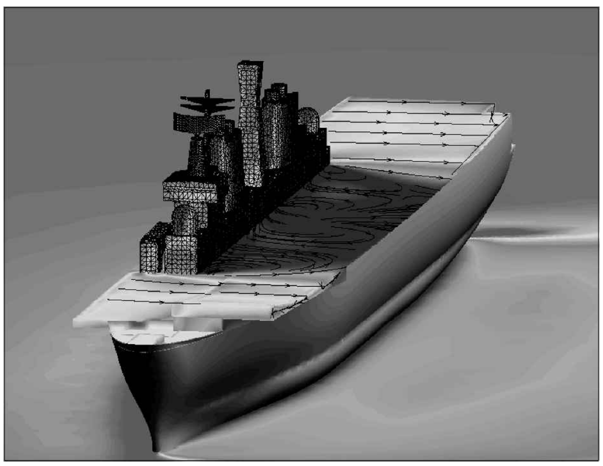

Fig. 13 Iso-Mach contours and selected streamlines on landing deck of the Ark Royal for α = 90 deg.

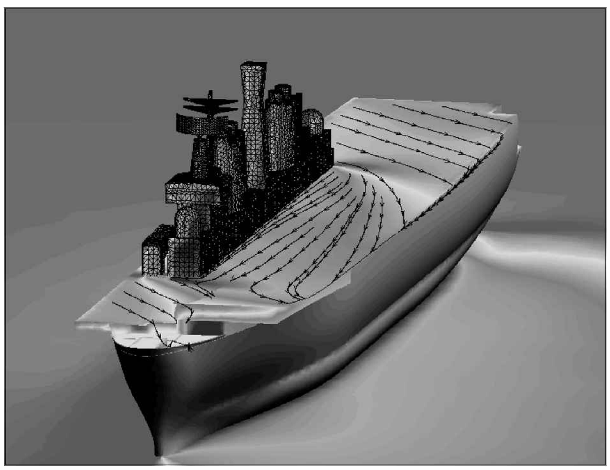

Fig. 14 Iso-Mach contours and selected streamlines on landing deck of the Ark Royal for α = 135 deg.

the outer flowfield. Thus, all unfavorable wind directions and unsafe landing conditions have been clearly identified for the simulator.

C. Ark Royal

Similar observations can be made for the Ark Royal, although the obstruction to the flow is only confined to the control tower section. It is therefore expected that the vortices will be of lesser intensity. Two results are presented for different wind directions: $\alpha = 90$ deg (Fig. 13) and $\alpha = 135$ deg (Fig. 14). The flow on the landing deck shows a similar behavior as on the Argus for the corresponding angle of attack: the wake of the control tower section sheds two counter-rotating vortices. Similarly, for $\alpha = 135$ deg no vortex structures are present.

D. LPH Ocean

The results for the LPH Ocean are presented in Figs. 15 and 16. (Here, a representation of the solution for all wind directions is shown, but, for brevity, only wind angles that requires more attention

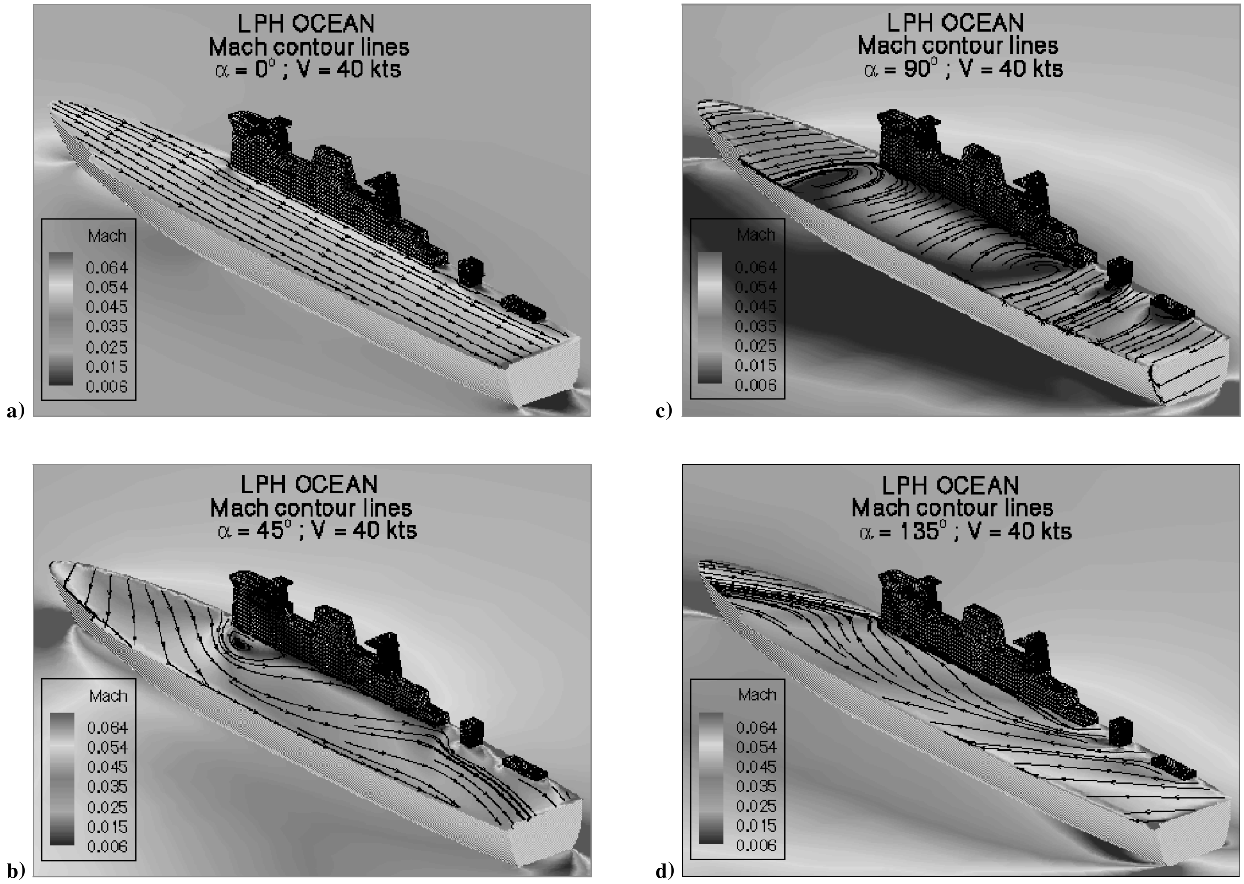

Fig. 15 Iso-Mach contours and selected streamlines of the LPH OCEAN at different wind directions.

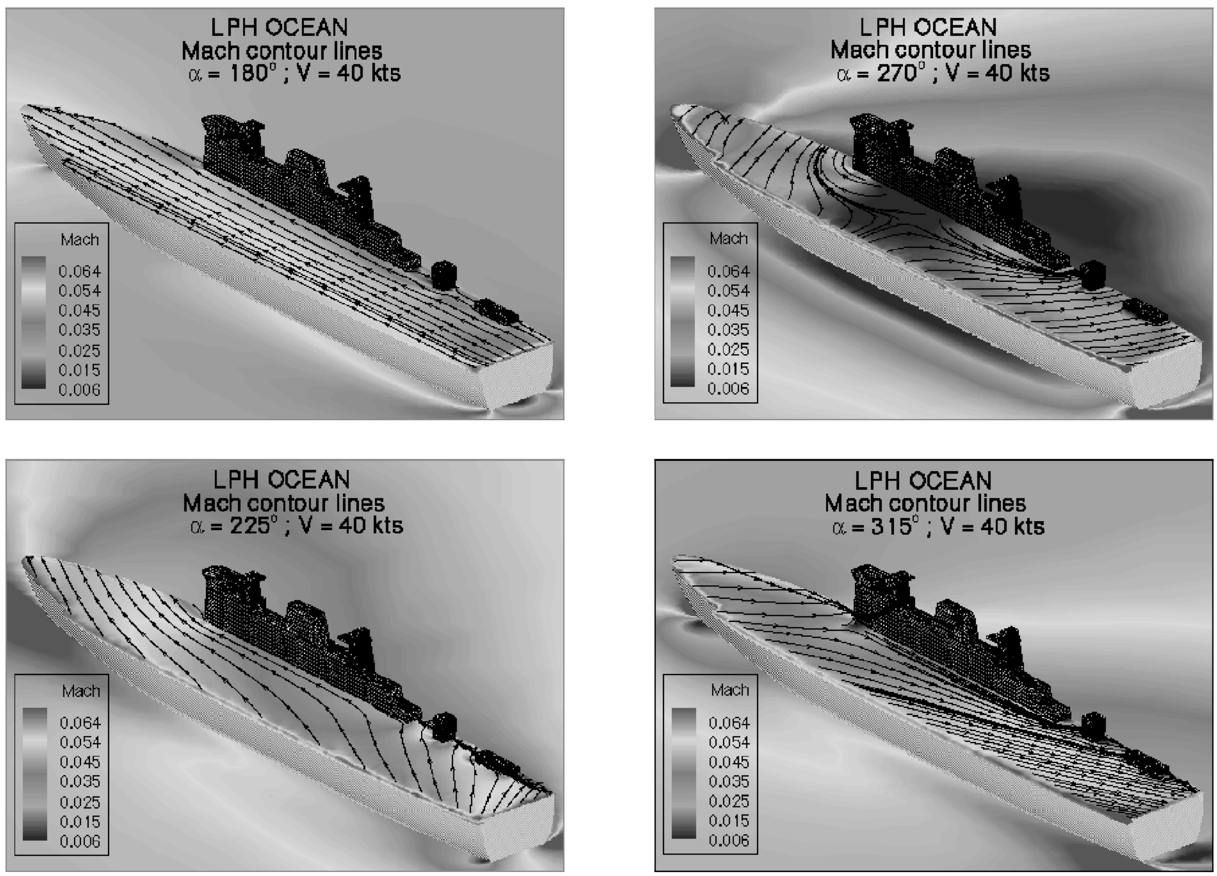

Fig. 16 Iso-Mach contours and selected streamlines of the LPH OCEAN at different wind directions.

will be discussed.) Because the LPH Ocean is an asymmetric ship and because the landing deck is along one side and the superstructures of the ship are on the opposite side, the results how that special attention should be given to the cases with angles of attack of 45 through 135 deg.

As can be seen from Fig. 15b, for a wind angle of 45 deg a small vortex is shed from the front superstructure, whereas at a wind angle of 90 deg (Fig. 15c) two bigger counter-rotating vortices are found to cover most of the middle section of the landing deck. Such vortex structures could create hazardous landing conditions for helicopter pilots.[2]

VI. Merlin Flight Simulator

This section describes the process of implementing the aerodynamic databases on the flight simulator built at CAE and the methods used to evaluate the CFD solutions from a training perspective. General information about other attempts for a CFD or empirical database for airwakes can be found in Refs. 6–12.

A. Simulator and Training Requirements

The CFD solutions were implemented on the Merlin full flight simulator. The simulator has a six-deg-of-freedom motion base, a three-deg-of-freedom vibration platform, a dynamic 7 and a 210 by 90-deg-field-of-view visual system. The helicopter flight simulator is shown in Figs. 17 and 18. The primary intent of the simulator is to train pilots for maritime warfare and search-and-rescue operations, which includes landing on the decks of various Royal Navy ships under realistic conditions. This requires the accurate modeling of helicopter performance, ship motion, sea state, and the effect of the winds around the ships' superstructures.

B. Data Reduction for the Merlin Simulator

Because unstructured meshes are not suitable for the purposes of an aerodynamic database, the results had to be interpolated onto a Cartesian grid. A six-block structure around the ship was defined and is represented in Figs. 19 and 20. For practical reasons block 1 was subdivided into six smaller blocks labeled 1a through 1f.

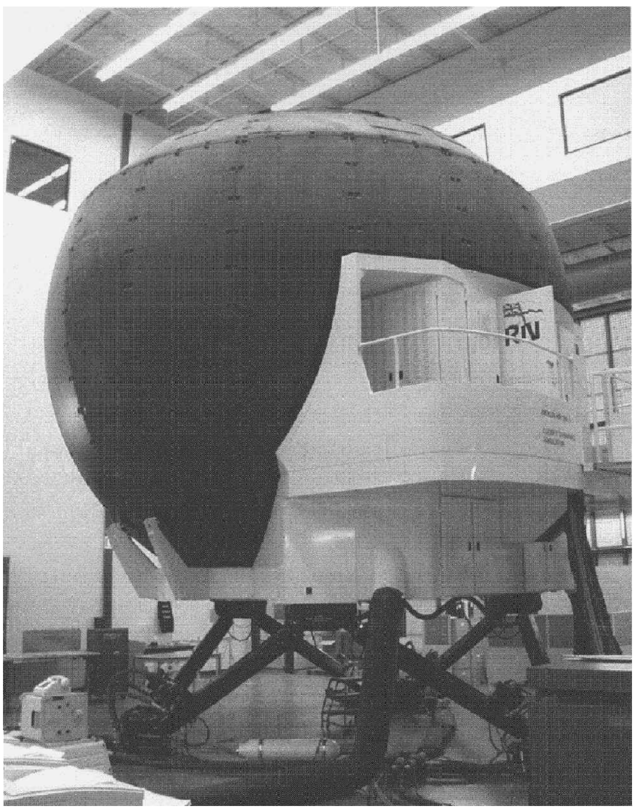

Fig. 17 View of the Merlin helicopter flight simulator.

Table 2 Block sizes and grid spacing on interpolated grid

Block	Length, $*L$	Width, $*b$	Height, $*h$	Grid Spacing, m
1	2	4	3	≤ 1
2	2	3	3	≤ 2
3	2	3	3	≤ 2
4	1	10	3	≤ 2
5	4	10	7	≤ 5
6	1	10	3	≤ 5

Fig. 18 Caption view from inside the Merlin helicopter flight simulator.

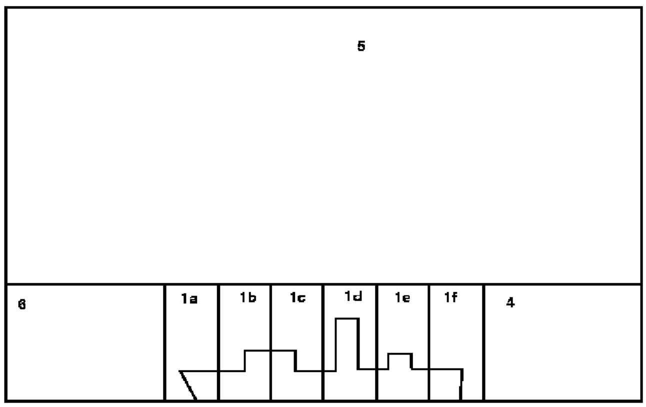

Fig. 19 Block structure around ship (side view) to define database look-up table points.

Another advantage of a block structure is that a better control of the grid density can be achieved in areas that are of interest from a helicopter's approach point of view (for example, higher grid density in the region of the wake of the ship). Table 2 gives the block sizes and grid spacing for the interpolated grid where L, b, and h represent the ship's length, width, and height, respectively.

C. Data Implementation Process

The data were incorporated directly into a three-dimensional look-up table. An algorithm was written to determine the location

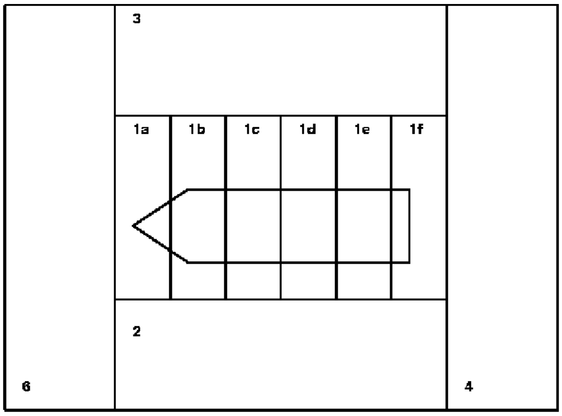

Fig. 20 Block structure around ship (top view) to define database look-up table points.

of each blade segment inside the flowfield and the relative speed and direction of the prevailing winds on the ship. Thus, the CFD flowfield ratio u/U_∞ was interpolated and used to determine the velocity at the blade segment. The process was executed at every frame of the blade element rotor model in order to capture as much of the flowfield characteristics as possible. The air-wake contribution was then added to the total blade segment velocity at each segment to compute the aerodynamic forces generated at each blade segment.

D. Evaluation Process

The evaluation process was made up of two steps. The first included running the CFD solution with the helicopter model in a stand-alone mode without a pilot in the loop. In this phase the main objective is to evaluate the correct implementation of the CFD database. The second step involved a pilot-in-the-loop evaluation of the database. The pilot is set up in an approach pattern and requested to perform a normal approach and landing at various wind speeds and directions. The pilot's control activity is monitored to determine the control margins and compared to the ship's SHOL (Ship Helicopter Operating Limits envelope). The pilot will then comment on the realism of the mission.

E. Results of the Implementation

Preliminary results show that the CFD solution captures the nature of the flow around the ships' superstructure quite realistically. A more extensive evaluation is under way to compare the SHOL of the CFD solution to that of the real aircraft and to evaluate the remaining wind directions. In the meantime the simulator has been built, accepted by the Royal Navy, and is utilized in the United Kingdom for helicopter training.

VII. Conclusions

CFD has been applied to the construction of a ship air-wake database. It is concluded that a combination of accurate Euler solutions and unsteadiness based on flow gradients might be sufficient for such purposes, in other words a Navier–Stokes solution could be overkill.

Several numerical milestones are crossed in applying the technology, not least among them is a thorough experimental validation that is carried out and shows excellent agreement between the calculations and the measurements, at several places on the ship.

The ultimate test however is the inclusion of the database and its acceptance by those who put their lives in danger landing on such decks. The overall feedback from pilots has been extremely positive, with the only criticism being in respect to the workload required in certain key areas. The workload has been modified by determining from the velocity field the relative intensity of turbulence and scaling it to meet the pilot's anticipated workload.

Future work will involve introducing the rotor downwash to see the effect it has on the flowfield. In addition, the use of CFD should be extended to determine the flowfield in other common simulator training exercises (that is, recirculation in confined areas, flow around buildings, etc.) and potentially to determine interference effects between a helicopter's main rotor downwash and the empennage.

References

[1]Habashi, W. G., "Putting Computers on Ice," *ICAO Journal*, Vol. 50, No. 7, 1995, pp. 14–17.

[2]Polsky, S. A., and Bruner, C. W. S., "Time-Accurate Computational Simulation of an LHA Ship Airwake," AIAA Paper 2000-4126, Aug. 2000.

[3]Bogstad, M. C., Habashi, W. G., Ait-Ali-Yahia, D., Metcalfe, L., Giannias, N., and Longo, V., "CFD Navy Ships Airwake Analysis for a Helicopter Flight Simulator," AIAA Paper 99-0996, Jan. 1999.

[4]Bogstad, M. C., Habashi, W. G., Giannias, N., and Longo, V., "CFD Ship Airwake Analysis for Helicopter Flight Simulators," National Research Council, TTCP AER-TP-2, May 1999.

[5]Baruzzi, G. S., Habashi, W. G., Guèvremont, J. G., and Hafez, M. M., "A Second Order Method for the Finite Element Solution of the Euler and Navier–Stokes Equations," *International Journal for Numerical Methods in Fluids*, Vol. 20, Feb. 1995, pp. 671–693.

[6]Zan, S. J., and Syms, G. F., "Numerical Prediction of Rotor Loads in an Experimentally-Determined Ship Airwake," National Research Council of Canada, Rept. LTR-AA-15, Ottawa, April 1995.

[7]Healey, J. V., "Establishing a Database for Flight in the Wake of Structures," *Journal of Aircraft*, Vol. 29, No. 4, 1992, pp. 559–564.

[8]Bollinger, W. K., "Visualization of the Flowfield Around a Generic Destroyer Model in a Simulated Turbulent Atmospheric Boundary Layer," M.S. Thesis, Rept. AD-A184658, Naval Postgraduate School, Monterey, CA, June 1987.

[9]Garry, E. A., "Aerodynamics Aspects of the Helicopter/Ship Interface—A Literature Survey," National Research Council of Canada, No. 32166, Ottawa, Oct. 1994.

[10]Carico, D., Reddy, B., and Dimarizio, C., "Ship Airwake Measurements and the Modeling Options for Rotorcraft Applications," Aircraft Ship Operations, AGARD CP509, Nov. 1991.

[11]Longobardi, R., Vismara, G., and Paggi, B., "EH101 Ship Interface Trials: Flight-Test Programme and Preliminary Results," Aircraft Operations, AGARD CP509, Nov. 1991.

[12]Landsberg, A. M., Boris, J. P., Sandberg, W., and Young, T. R., "Analysis of the Nonlinear Coupling Effects of a Helicopter Downwash with an Unsteady Airwake," AIAA Paper 95-0047, Jan. 1995.